LARGE EDDY SIMULATION OF TURBULENT PIPE FLOW

Murray Rudman and Hugh M. Blackburn

CSIRO Building, Construction and Engineering

Graham Rd, Highett, Victoria, AUSTRALIA

ABSTRACT

Results from a spectral element large eddy simulation of turbulent pipe flow are presented for a bulk flow Reynolds number of 36 700. The LES uses a Smagorinsky subgrid-scale stress model and, because the wall layers are resolved, van Driest-type wall damping is required. Although the geometry has cylindrical symmetry, Cartesian coordinates were employed, illustrating the potential of the method to model complex geometries with unstructured meshes. Simulation results compare favorably with experimental measurements at the same Reynolds number, demonstrating the possibility of performing large eddy simulation with the method in geometrically more complicated systems.

INTRODUCTION

Large Eddy Simulation (LES) has been used in computational fluid dynamics simulations since the pioneering work of Smagorinsky (1963). Despite being applied in turbulence simulations for at least as long as Reynolds-averaged (RANS) methods (Launder & Spalding 1971), it has only been widely used in meteorological applications (e.g. Mason & Thomson 1987, Mason 1994) and has had little impact in the process industries. There are three main reasons for this lack of utilisation of LES techniques. First, the often complicated nature of the physical systems involved in process industry applications means that turbulence closures may involve many equations with many unknown cross-correlations having to be modelled. Although this is also a significant problem in RANS closures, the time-averaged experimental measurements needed to estimate arbitrary model parameters are usually significantly easier to make than equivalent measurements needed to estimate parameters for unsteady, sub-grid scale turbulent cross-correlations. Second, the geometrically complicated nature of many process applications has meant that, unlike most meteorological applications, simple computational meshes cannot be used and body fitted grids, low-order finite-element and finite-volume discretisations must be applied. It is the low-order nature of these numerical schemes (at best second-order and often first) that precludes their use in successful LES. The numerical diffusion arising from many of these schemes is higher than the turbulent diffusion and dispersion errors arising from non-linear terms soon invalidate the simulation. Finally, the computational expense of LES is significant when compared to many RANS techniques.

The majority of LES of turbulent flows have been performed using either spectral methods, finite difference methods or mixed spectral/finite difference methods. As a result, they have been restricted to simple geometries. Spectral element spatial discretisations hold promise for LES of turbulent flows in complex geometries because of the method's ability to provide arbitrary geometric complexity and high accuracy with low numerical diffusion and dissipation. Despite this, spectral element methods have not yet been widely employed for LES.

This paper documents results from a spectral element LES of turbulent pipe flow. Turbulent pipe flow has not been investigated as extensively as its Cartesian equivalent, turbulent channel flow, although some work has appeared (Unger & Friedrich 1991, Eggels 1994, Orlandi & Fatica 1997). Despite the comparatively simple geometry, the presence of a singularity on the axis in cylindrical coordinates gives rise to numerical difficulties not present in channel flow. This singularity is removed in the current work by using Cartesian coordinates and a spectral element discretisation in planes perpendicular to the pipe axis and Fourier expansions in the axial direction. This may be considered an example of a 'complex' geometry for Cartesian coordinates and serves as an illustration of the ability of the method to tackle more complex geometries applicable to industrial applications.

A bulk flow Reynolds number of 36 700 was chosen for which experimental data is available (Lawn 1971). For this Reynolds number, the dimensionless wall shear stress (non-dimensionalised by bulk flow velocity, pipe diameter and fluid velocity) is $\tau_w = 0.00284$ and the non-dimensional wall friction velocity $u_\tau = (\tau_w/\rho)^{1/2}$ is 0.053. Based on u_τ and the pipe diameter D, the friction Reynolds number corresponds to $Re_\tau = u_\tau D/\nu = 1920$.

LES METHODOLOGY

In large eddy simulation, an attempt is made to capture the large scale unsteady motions which carry the bulk of the mass, momentum and energy in a flow. The length scale on

which these 'resolved scale' motions occur depends primarily on the local mesh resolution. The small scale motions that occur on length scales smaller than the mesh spacing cannot be captured and their effects on the resolved scale motions must be modelled. Because less of the flow is being modelled in LES than in RANS calculations, it is hoped that the models will be more accurate as well as simpler to formulate. Whether or not this hope is justified is not clear at the current time.

Mathematically, the LES procedure can be thought of as a convolution of the exact turbulent velocity field u with a filter function K that gives the resolved scale velocity field $\overline{u}$,

$$\overline{u}(r) = \int K(\Delta, |r - r'|)\, u(r')\, \mathrm{d}^3 r'. \tag{1}$$

The filtering operation is implicit in the formulation (i.e. not explicitly carried out). Under assumptions which are generally non-restrictive (see e.g. Leonard 1974), filtering and differentiation commute, i.e. $\overline{\partial u/\partial x} = \partial \overline{u}/\partial x$.

An equation for $\overline{u}$ is obtained by convolving the Navier-Stokes equations with the same spatial filter function,

$$\frac{\partial \overline{u}}{\partial t} + \nabla \cdot \overline{uu} = -\nabla \overline{P} + \nu \nabla^2 \overline{u}, \tag{2}$$

where $P = p/\rho$ for a constant density flow. As in conventional turbulence modelling, the nonlinear terms are not closed, because the filtered non-linear terms $\overline{uu}$ cannot be written in terms of the known resolved components $\overline{u}$. To overcome this problem, a subgrid-scale stress (SGSS) τ is introduced (in a similar way to RANS modelling), such that $\overline{uu} = \overline{u}\,\overline{u} + \tau$. The momentum equation then becomes

$$\frac{\partial \overline{u}}{\partial t} + \nabla \cdot \overline{u}\,\overline{u} = -\nabla \overline{P} + \nu \nabla^2 \overline{u} - \nabla \cdot \tau. \tag{3}$$

The turbulence modelling task is to estimate the subgrid-scale stress τ from the resolved velocity field $\overline{u}$.

SGSS model

The simplest SGSS models are of the eddy viscosity type, with the Smagorinsky mixing length model (Smagorinsky 1963) the most well known. It is used in this study. In eddy viscosity models, it is assumed that the anisotropic part of τ is related to the resolved strain rate field through a scalar eddy viscosity,

$$\tau - \frac{1}{3}\,\mathrm{tr}(\tau)\mathbf{1} = -2\nu_t \overline{S} = -\nu_t \left[\nabla \overline{u} + (\nabla \overline{u})^t\right], \tag{4}$$

with the isotropic part of τ being subsumed in P.

In the Smagorinsky model, the turbulent eddy viscosity is written as

$$\nu_t = (C_S \Delta)^2 2^{1/2}\, |S| = (C_S \Delta)^2\, \mathrm{tr}(2\overline{S}^2)^{1/2}, \tag{5}$$

where S is the second invariant of the rate-of-strain tensor, C_S is a model constant and $\Delta = (\Delta x \Delta y \Delta z)^{1/3}$ is a measure of the local grid length scale which varies spatially in the application here.

Wall treatment

Rather than use a wall-function approach to the treatment of solid boundaries, the near-wall regions of the flow are resolved in the simulations reported here by ensuring sufficiently fine mesh spacing. In such cases it has been shown that the eddy-viscosity must be modified using a wall damping which switches off the eddy viscosity in the near-wall region.

A common model is van Driest damping, and a form which gives the correct near-wall asymptotic behaviour of the SGS stresses is that introduced by Piomelli, Ferziger & Moin (1987), where the turbulent mixing length $C_S \Delta$ is modified using

$$C_S \Delta \left[1 - \exp(-(r^+/A^+)^3)\right]^{1/2}, \tag{6}$$

with r^+ as the dimensionless wall-normal distance $(R - r)/(u_\tau/\nu)$ and the constant $A^+ = 26$. The damping only has significant effect for $r^+ < 40$. Note that this approach requires that the mean wall shear stress be known in order to determine $r^+ = (R - r)u_\tau/\nu$. This does not present a problem in the present application, as the time-mean wall shear stress can be determined from the Blasius friction factor for turbulent pipe flow. In more general cases, this approach would be difficult to implement as u_τ would not be known in advance.

NUMERICAL TECHNIQUE

The spatial discretisation employs a spectral element/Fourier formulation, which allows arbitrary geometry in the (x, y) plane, but requires periodicity in the z (out-of-plane) direction. The basis of the method as applied to DNS of the incompressible Navier–Stokes equations has been described by Karniadakis & Henderson (1998). The nonlinear terms of (3) have been implemented here in skew-symmetric form, i.e. $(\overline{u} \cdot \nabla \overline{u} + \nabla \overline{u}\,\overline{u})/2$, because this has been found to reduce aliasing errors.

The method described in Karniadakis & Henderson requires modification in order to deal with the $\nabla \cdot \tau$ terms in (3). The approach taken here follows that outlined in Karnidakis, Orszag & Yakhot (1993), where the sum of the molecular and turbulent eddy viscosities $\nu_T = \nu_t + \nu$ is decomposed into a spatially-constant component ν_{ref} and a spatially-varying component $\nu_T - \nu_{\mathrm{ref}}$. The value of ν_{ref} is chosen to be approximately equal to the maximum value of ν_T. This value is not known *a priori*, but ν_{ref} can be adjusted during the computation without any adverse effects. When solving (3), the term $\nabla \cdot (\nu_T - \nu_{\mathrm{ref}}) \left[\nabla \overline{u} + (\nabla \overline{u})^t\right]$, is treated explicitly, while the term $\nu_{\mathrm{ref}} \nabla^2 \overline{u}$, is treated implicitly, thus enhancing the overall numerical stability of the scheme.

In order to drive the flow in the axial (z) direction, a body force per unit mass of magnitude $2\tau_w/R\rho$ was applied to the z-component of (3). This approach allows the pressure to be periodic in the streamwise direction.

As a result of the Fourier decomposition, implementation of the time integration as a parallel algorithm is straight-
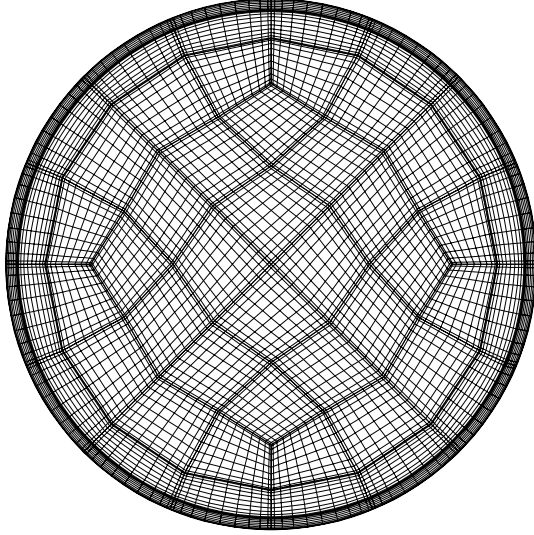
Figure 1: A two-dimensional section of the 64-element mesh. The elements near the pipe wall are shrunk in the radial direction to ensure sufficient near-wall resolution. For Re=37 600, the first mesh point is at a position given by $r^+ \approx 1$.

forward, with inter-process communication required only during formulation of the nonlinear terms in (3). The message-passing kernel MPI has been used for this operation, and the computations reported here were carried out using eight processors on an NEC SX4-32 supercomputer.

Mesh parameters

The computational mesh is chosen on the basis that the size of the domain represented is 'sufficiently large', with the mesh spacing decided by resolution requirements.

In the pipe flow geometry, the streamwise dimension (which is treated assuming periodicity) is usually based on the integral correlation lengths of turbulence, as obtained from physical experiment. A length of $L_z = 5D$ was used in Eggels (1994) and found to be adequate. Here, a value of $L_z = 2\pi D$ is chosen.

An important consideration for wall resolving LES is the mesh spacing near the wall. According to the recommendations of Piomelli (1997) for wall-resolving LES, the first mesh point away from the wall should be located at $r^+ < 1$. The streamwise mesh spacing should satisfy $\Delta z^+ \simeq 50$–100, and the azimuthal mesh spacing at the pipe wall should satisfy $R\Delta\theta^+ \simeq 15$–$40$. For the mesh here, 10th order elements were used with 192 Fourier modes in the axial direction. This leads to values of $r^+ \approx 1$ for the first mesh point away from the pipe wall, $\Delta z^+ \approx 75$ and $R\Delta\theta \approx 45$ at the pipe wall. The corresponding two-dimensional mesh is shown in figure 1 and there are approximately 1.2 million mesh points in the three-dimensional domain.

The Smagorinsky constant is the only adjustable parameter in the current simulation. Values as high as 0.2 have been used in simulations of isotropic turbulence (Smagorinsky 1963) compared to 0.1 in pipe flow simulations (Eggels 1994) and $C_S = 0.065$ in channel flow simulations. Values of 0.065 and 0.1 are chosen here, and the effect of modifying this constant is discussed. The local mesh lengths Δx, Δy used to compute Δ were evaluated by dividing the local element lengths by the order of the tensor-product shape functions, i.e. $(np - 1)$ where $np = 11$ is the number of mesh points along an element edge. The streamwise mesh spacing is $\Delta z = 2\pi/192 = 0.0327$.

Suitable initialisation of the flow proved to be difficult. Initial attempts involved setting a laminar pipe flow with the correct volumetric flow rate and a pressure gradient (implemented as a body force) appropriate for the turbulent flow. When small perturbations were added to this base flow, they rapidly decayed as the pressure gradient accelerated the base flow. Successful initialisation was eventually performed at a low resolution using a laminar pipe flow, but assuming a pressure gradient appropriate for the turbulent flow (i.e., the volumetric flow was too high). A small perturbation was added to this base flow and rapidly grew. As the magnitude of the fluctuations increased, the grid resolution was increased in increments to the final values mentioned above.

All mean flow quantities discussed below were gathered after the flow had reached statistical equilibrium. Time averaging was undertaken for a time approximately equal to the time taken for the mean flow to traverse the computational domain twice.

RESULTS

Mean velocity

Mean velocity profiles are displayed in figure 2 in wall units: $U^+ = u/u_\tau$, $r^+ = (R - r)u_\tau/\nu$. For comparison purposes the $Re_c = 24\,600$ experimental results of den Toonder & Nieuwstadt (1997) are shown, along with a 'Law of the Wall' plot which uses $U^+ = 5.0 + 2.5\ln r^+$ in the logarithmic region.

It can be seen that results using $C_S = 0.1$ provide a good match between the computation and the 'Law of the Wall'. They also provide a close match to the experimental results of den Toonder & Nieuwstadt (1997), from the viscous sublayer through the buffer region, log layer and into the core region of the pipe flow. Although these experimental results are for a bulk flow Reynolds number of 24 600, by this Reynolds number the profiles reported by den Toonder & Nieuwstadt (in wall coordinates) had ceased to change in the buffer layer and log region. The results for $C_S = 0.065$ under-predict the axial velocity in the log region and slightly over-predict it in the core flow. The value $C_S = 0.065$ has previously been shown to be the optimal value for channel flow (e.g. Blackburn 1998). The results here suggest $C_S = 0.1$ is optimal for pipe flow. Thus the Smagorinsky constant needs to be tuned for the flow under investigation, which is a weakness shared by many RANS models. The deficien-
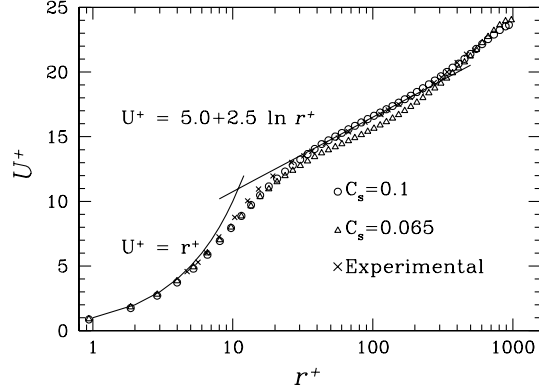
Figure 2: Mean velocity profiles. ——, Law of the Wall; $\times$, Experimental results of den Toonder & Nieuwstadt at Re=24 600; $\circ$, Numerical results with $C_S = 0.1$; $\triangle$, Numerical results with $C_S = 0.065$.

cies of simple turbulence models with adjustable constants are clearly highlighted.

Velocity fluctuations

The resolved-scale r.m.s velocity fluctuations (normalised by the friction velocity, u_τ) from the LES results are compared with the experimental measurements of Lawn (1971), at the same Reynolds number, in figure 3.
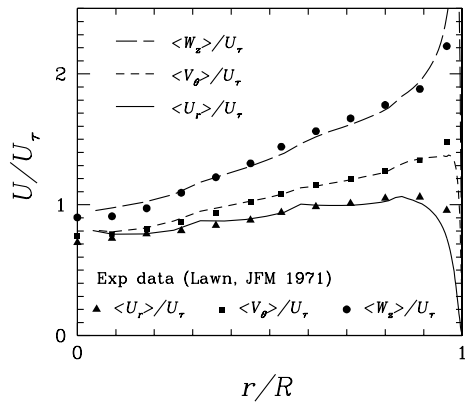

Figure 3: Resolved scale fluctuating velocity components normalised by the friction velocity, U_τ. The lines are for results calculated here and the symbols are results presented in Lawn for the same Reynolds number.

It can be seen that agreement is good, although there are two points worth mentioning. First, the sub-grid scale contributions to the r.m.s. velocity components have not been taken into account in the LES results, and if done so, they would increase the LES results slightly. Second, there is a noticeable 'lumpiness' to the LES profiles, especially for

the radial velocity component. This lumpiness is associated with the location of element boundaries, and illustrates one problem with the current numerical method when used for LES simulation. The computed solutions using a spectral element method have C^0 continuity at element boundaries, and thus derivatives may be discontinuous on opposite sides of an element boundary node. As the spatial resolution improves and all flow features are resolved, the errors associated with this lack of C^1 continuity decrease. However, the underlying assumption in LES is that the flow is not fully resolved and thus discontinuities in derivatives at element boundaries may contribute to exaggerated estimates of eddy viscosity and other effects of an unphysical nature. Although this may be an important issue in obtaining accurate estimates of high-order turbulence statistics, it appears to have less of an impact for quantities such as mean velocity and is unlikely to lessen the utility of the method in applications.

Reynolds shear stress

Figure 4 compares the predicted mean resolved-scale Reynolds shear stress profile with the experimental results of Lawn (1971) at the same Reynolds number. The results
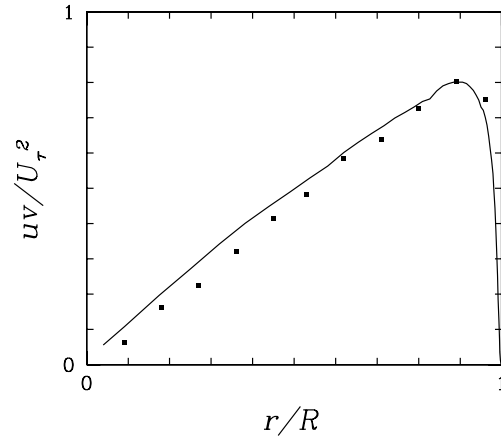

Figure 4: Resolved scale Reynolds shear stress. The solid line are LES results and the symbols are experimental values of Lawn.

are in reasonable agreement, although the LES results over-predict the Reynolds shear stress by up to 25% near the pipe centerline. As with the r.m.s. velocity fluctuations, the effect of the spectral element discretisation can be seen in the slight lumpiness of the profile.

Qualitative flow features

An instantaneous cross section of the flow in one quadrant is presented in Figure 5. The unsteadiness in the flow can clearly be inferred from the significant amount of small-scale structure visible in this image. Also seen at the
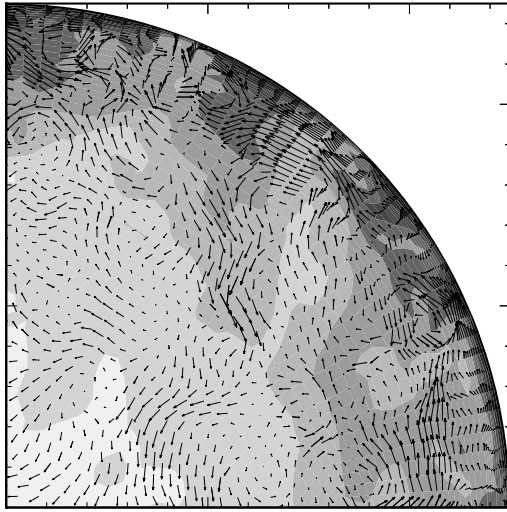
Figure 5: Contours of instantaneous streamwise velocity and in-plane velocity vectors in one quadrant of the pipe flow.

1 O'clock position near the wall is an ejection event (dark contour region with in-plane velocity vectors directed away from the wall) which results in a low-speed streak in the boundary layer.

These streaks are also clearly seen in Figure 6 which shows contours of streamwise velocity on the pipe wall at $r^+ \approx 20$. From these results, a mean spacing of the wall streaks is estimated to be approximately 150 wall units, although the two-point correlations that would quantify this more accurately are yet to be performed.

A contour of the fluctuating component of the out-of-plane velocity in a plane through the pipe centerline is shown in Figure 7. Superimposed on top of the small-scale turbulence in the core region of the flow, large scale structure, on the scale of the pipe diameter, is clearly seen. Near the pipe walls, (the left and right sides of Figure 7) the ejection events described earlier are seen as the light and dark regions that leave the pipe walls at an angle of approximately 15–20°.

DISCUSSION

The results obtained from a spectral element LES simulation of turbulent pipe flow are seen to be in good agreement with experimental measurements at the same Reynolds number. These results indicate that spectral element techniques can be employed for LES in complex geometries using unstructured meshes and attain a good degree of success. The results predicted here are similar to those obtained with more standard finite difference/volume discretisation schemes with a similar number of mesh points (e.g. approximately 800 000 mesh cells were used in the LES simulations of Eggels 1994). The simulation of the cylindrical
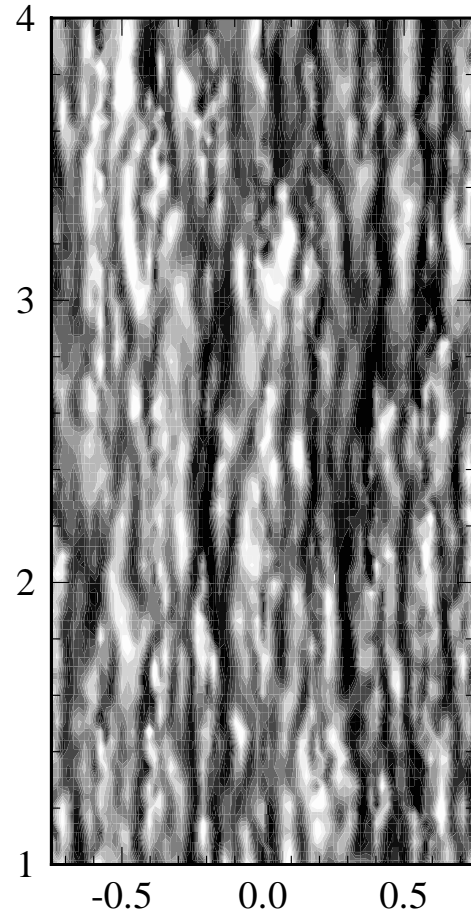

Figure 6: Contours of instantaneous streamwise velocity at $r^+ \approx 20$. The flow is from bottom to top and only half of the pipe-wall is shown, projected onto a flat surface.

pipe geometry in a Cartesian coordinate system gives a clear demonstration of the method's ability to simulate non-trivial geometries. However, with the current method an *a priori* knowledge of the wall shear stress is required and the most important development that remains to be undertaken is the implementation of sub-grid scale stress models that do not require this.

Although flows such as pipe flow are geometrically simple, their accurate simulation at high Reynolds numbers using techniques such as LES are in some ways more difficult than flows in complicated geometries. Unsteadiness, the transition to turbulence and its subsequent maintenance in pipe flow are due to hydrodynamic instability alone, and any numerical scheme that simulates this flow must have high accuracy with low numerical diffusion and dispersion. In contrast, in many process applications, unsteadiness and subsequent generation of turbulence is a result of entry flows (jets, pipes, nozzles, etc.) or vortex shedding from solid surfaces (impellers, baffles, etc.). In these latter flows, there is an on-going source of unsteadiness that will assist in the onset and maintenance of turbulence in a numerical simulation. Because such sources are absent from pipe flow, its accurate
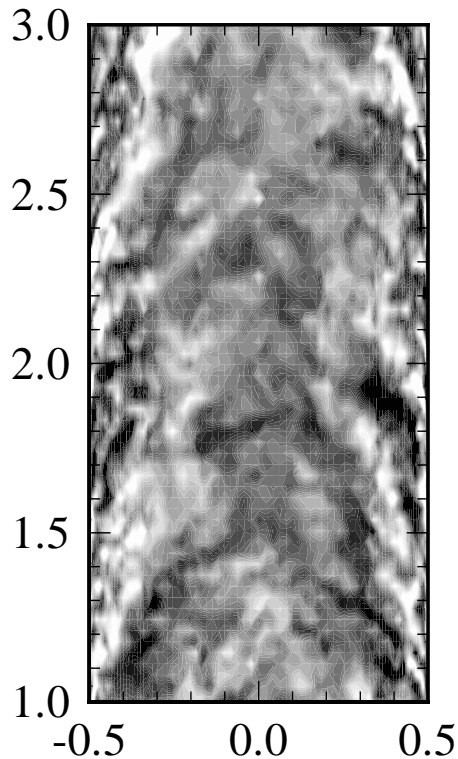
Figure 7: Contours of instantaneous out-of-plane velocity in a plane through the pipe centerline.

simulation is an indication of the reliability of the method.

REFERENCES

BLACKBURN, H. M. (1998). Channel flow LES with spectral elements, *13th Australasian Fluid Mechanics Conference*, Monash University.

DEN TOONDER, J. M. J. & NIEUWSTADT, F. T. M. (1997). Reynolds number effects in a turbulent pipe flow for low to moderate re, *Phys. Fluids* **9**: 3398–3409.

EGGELS, J. G. M. (1994). *Direct and large eddy simulation of turbulent flow in a cylindrical pipe geometry*, Delft University Press, Delft, The Netherlands. Ph.D. Thesis of Jack Eggels.

KARNIADAKIS, G. E. & HENDERSON, R. D. (1998). Spectral element methods for incompressible flows, *in* R. W. Johnson (ed.), *Handbook of Fluid Dynamics*, CRC Press, Boca Raton, chapter 29, pp. 29–1–29–41.

KARNIDAKIS, G. E., ORSZAG, S. A. & YAKHOT, V. (1993). Renormalization group theory simulation of transitional and turbulent flow over a backward-facing step, *in* B. Galperin & S. A. Orszag (eds), *Large Eddy Simulation of Complex Engineering and Geophysical Flows*, Cambridge, chapter 8, pp. 159–177.

LAUNDER, B. E. & SPALDING, D. B. (1971). The numerical computation of turbulent flow, *Comp. Meth. in Appl. Mech. Eng.* **3**: 269.

LAWN, C. J. (1971). The determination of the rate of dissipation in turbulent pipe flow, *J. Fluid Mech.* **48**: 477–505.

LEONARD, A. (1974). Energy cascade in large-eddy simulations of turbulent fluid flows, *Adv. Geophys* **18**: 237–248.

MASON, P. J. (1994). Large eddy simulation: A critical review of the technique, *Q. J. R. Meteorol. Soc.* **120**: 1–26.

MASON, P. J. & THOMSON, D. J. (1987). Large-eddy simulations of the neutral-static-stability planetary boundary layer, *Q. J. R. Meteorol. Soc.* **113**: 413–443.

ORLANDI, P. & FATICA, M. (1997). Direct simulations of turbulent flow in a pipe rotating about its axis, *J. Fluid Mech.* **343**: 43–72.

PIOMELLI, U. (1997). Large-eddy simulations: Where we stand, *in* C. Liu & Z. Liu (eds), *Advances in DNS/LES*, AFOSR, Louisiana, pp. 93–104.

PIOMELLI, U., FERZIGER, J. H. & MOIN, P. (1987). Models for large eddy simulations of turbulent channel flows including transpiration, *Technical Report TF-32*, Department of Mechanical Engineering, Stanford University.

SMAGORINSKY, J. S. (1963). General circulation experiments with the primitive equations, *Monthly Weather Rev.* **91**: 99–164.

UNGER, F. & FRIEDRICH, R. (1991). Large eddy simulation of fully-developed turbulent pipe flow, *Eighth Symposium on Turbulent Shear Flows, Munich, Germany*.